COMPDYN 2011
ECCOMAS Thematic Conference on
Computational Methods in Structural Dynamics and Earthquake Engineering
M. Papadrakakis, M. Fragiadakis, V. Plevris (eds.)
Corfu, Greece, 25-28 May 2011

FUZZY AND FUZZY STOCHASTIC METHODS FOR THE NUMERICAL ANALYSIS OF REINFORCED CONCRETE STRUCTURES UNDER DYNAMICAL LOADING

F. Steinigen[1], **J.-U. Sickert**[1], **W. Graf**[1] **and M. Kaliske**[1]

[1]Technische Universität Dresden
Institute for Structural Analysis
01062 Dresden, Germany
e-mail: frank.steinigen@tu-dresden.de

Keywords: Structural Dynamics, Reinforced Concrete, Fuzzy Stochastic Analysis.

Abstract. *This paper is mainly devoted to enhanced computational algorithms to simulate the load-bearing behavior of reinforced concrete structures under dynamical loading. In order to take into account uncertain data of reinforced concrete, fuzzy and fuzzy stochastic analyses are presented. The capability of the fuzzy dynamical analysis is demonstrated by an example in which a steel bracing system and viscous damping connectors are designed to enhance the structural resistance of a reinforced concrete structure under seismic loading.*

1 INTRODUCTION

The numerical analysis of reinforced concrete (RC) structures under dynamical loads requires realistic nonlinear structural models and computational algorithms. Furthermore, the engineer/designer has to deal with uncertainty which result from variations in material parameters as well as incomplete knowledge about further excitations and the quality of the numerical model itself. The variations in material parameters may be assessed by the uncertainty measure probability. However, the stochastic model cannot be determined precisely because of rare information in most cases. Therefore, an imprecise probability approach is suggested in this contribution bases on the uncertainty measure fuzzy probability resulting in a set of probability models which assessed by membership values. Using this approach, input variables may be also modeled as fuzzy quantities and considered as a special case, if only subjective or linguistic assessments are available.

The incorporation of uncertain input variables within a dynamic structural analysis leads to uncertain structural responses representing the uncertain structural performance close to reality. The uncertain structural responses are determined using fuzzy stochastic dynamic analysis. Thereby, fuzzy stochastic processes result because of the specific dynamic actions. The fuzzy stochastic structural analysis of practical problems requires high performance computational tools in order to deal with a large number of uncertain input variables as well as complex nonlinear structural models. An efficient approach is introduced which is based on α-level optimization and Monte-Carlo simulation using meta-models which partly replace the dynamic structural analyses.

2 UNCERTAINTY IN STRUCTURAL DYNAMICS

2.1 Data models

The input variables – for geometry, material, load etc. – of the numerical simulations of structural behavior are generally uncertain. To describe this uncertainty, traditional stochastic and non-stochastic models are available [6]. In Fig. 1, the models randomness, fuzziness and fuzzy randomness are displayed. The choice of the model depends on the available data.

If sufficient statistical data exist for a parameter and the reproduction conditions are constant, the parameter may be described stochastically. Thereby, the choice of type of probability distribution function affects the result considerably.

Overcoming the traditional probabilistic uncertainty model enables the suitable consideration of imprecision (epistemic uncertainty). Thereby, epistemic uncertainty is associated with human cognition, which is not limited to a binary measure. Advanced uncertainty concepts allow a gradual assessment of intervals. This extension can be realized with the uncertainty characteristic fuzziness. The combination of fuzziness and probabilistic leads to the generalized model fuzzy randomness.

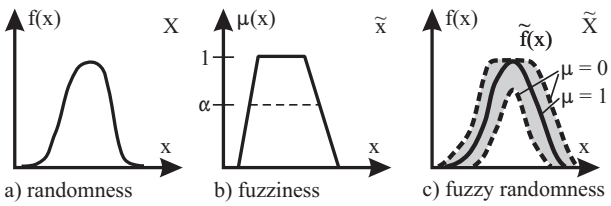

Figure 1: Models of uncertainty.

2.1.1 Fuzzy variables

Often, the uncertainty description for parameters is based on pure expert judgment or samples which are not validated statistically. Then, the description by the uncertainty model fuzziness is recommended. The model comprehends both objective and subjective information. The uncertain parameters are characterized with the aid of a membership function $\mu(x)$ (see Fig. 1b) and Eq. (1)). The membership function $\mu_x(x)$ assesses the gradual membership of elements to a set. Fuzzy variables

$$\tilde{x} = \{(x;\, \mu_x(x)) \mid x \in X\}; \quad \mu_x(x) \geq 0 \,\forall\, x \in X \tag{1}$$

may be utilized to describe the imprecision of structural parameters directly as well as to specify the parameters of fuzzy random variables.

2.1.2 Fuzzy random variables

If, e.g. reproduction conditions vary during the period of observation or if expert knowledge completes the statistical description of data, an adequate uncertainty quantification succeeds with fuzzy random variables. The theory of fuzzy random variables is based on the uncertain data model fuzzy randomness representing a generalized model due to the combination of stochastic and non-stochastic characteristics. A fuzzy random variable $\tilde{X}$ is defined as the fuzzy set of their originals, whereby each original is a real-valued random variable X.

The representation of fuzzy random variables presented in this paper is based on [12]. The space of the random elementary events Ω is introduced. Here, e.g. the measurement of a structural parameter may be an elementary event ω. Each elementary event $\omega \in \Omega$ generates not only a crisp realization but a fuzzy realization $\tilde{x}(\omega) = \tilde{x}$, in which $\tilde{x}$ is an element of the set $\mathbf{F}(\mathbb{R})$ of all fuzzy variables on $\mathbb{R}$. Each fuzzy variable is defined as a convex, normalized fuzzy set, whose membership function $\mu_x(x)$ is at least segmentally continuous. Accordingly, a fuzzy random variable $\tilde{X}$ is a fuzzy result of the mapping given by

$$\tilde{X} : \Omega \mapsto \mathbf{F}(\mathbb{R}). \tag{2}$$

Based on this formal definition, a fuzzy random variable is described by its fuzzy cumulative distribution function (fuzzy cdf) $\tilde{F}(x)$. The function $\tilde{F}(x)$ is defined as the set of real-valued cumulative distribution functions F(x) which are gradually assessed by the membership $\mu_F(F(x))$. F(x) is the cdf of the original X and is referred to as trajectory of $\tilde{F}(x)$. As result, a fuzzy functional value $\tilde{F}(x_i)$ belongs to each value x_i (see Fig. 2). Thus, $\tilde{F}(x)$ represents a fuzzy function as defined in Section 2.2.1. A fuzzy probability density function

$$\tilde{f}(x) = \{(f(x);\, \mu_f(f(x))) \mid f \in \mathbf{f}\}; \quad \mu_f(f(x)) \geq 0 \;\forall\; f \in \mathbf{f} \tag{3}$$

is defined accordingly. In that, $\mathbf{f}$ represents the set of all probability density functions defined on X.

2.2 Uncertain functions and processes

2.2.1 Fuzzy function

In case that fuzzy parameters depend on crisp or uncertain conditions, they are modeled as fuzzy functions $\tilde{x}(\underline{\tilde{t}}) = \tilde{x}(\underline{\tilde{\theta}}, \tilde{\tau}, \underline{\tilde{\varphi}})$ or in the special case of pure time dependency as fuzzy

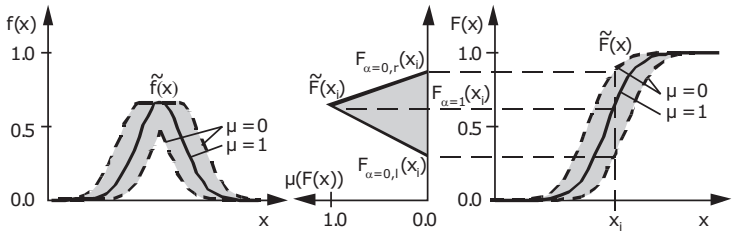

Figure 2: Fuzzy probability density and cumulative distribution function.

processes $\tilde{x}(\tilde{\tau})$. Arguments may be the time $\tilde{\tau}$, the spatial coordinates $\underline{\tilde{\theta}}$ and further parameters $\underline{\tilde{\varphi}}$, e.g. temperature. A fuzzy function $\tilde{x}(\underline{\tilde{t}})$ enables the formal description of at least piecewise continuous uncertain structural parameters in $\mathbb{R}$. In the following, a definition of fuzzy functions is introduced. Given are

- the fundamental sets $\mathbf{T} \subseteq \mathbb{R}$ and $\mathbf{X} \subseteq \mathbb{R}$,
- the set **F(T)** of all fuzzy variables $\underline{\tilde{t}}$ on the fundamental set **T**,
- the set **F(X)** of all fuzzy variables $\tilde{x}$ on the fundamental set **X**.

Then, the uncertain mapping of **F(T)** into **F(X)** that assigns exactly one $\tilde{x} \in \mathbf{F}(\mathbf{X})$ to each $\underline{\tilde{t}} \in \mathbf{F}(\mathbf{T})$ is referred to as a fuzzy function denoted by

$$\tilde{x}(\underline{\tilde{t}}): \quad \mathbf{F}(\mathbf{T}) \tilde{\mapsto} \mathbf{F}(\mathbf{X}), \tag{4}$$

$$\tilde{x}(\underline{\tilde{t}}) = \left\{ \tilde{x}_t = \tilde{x}(\underline{\tilde{t}}) \quad \forall\, \underline{\tilde{t}} \mid \underline{\tilde{t}} \in \mathbf{F}(\mathbf{T}) \right\}. \tag{5}$$

In Fig. 3, a fuzzy process $\tilde{x}(\tau)$ is presented, which assigns a fuzzy quantity $\tilde{x}(\tau_i)$ to each time τ_i. For the numerical simulation, a bunch parameter representation of a fuzzy function

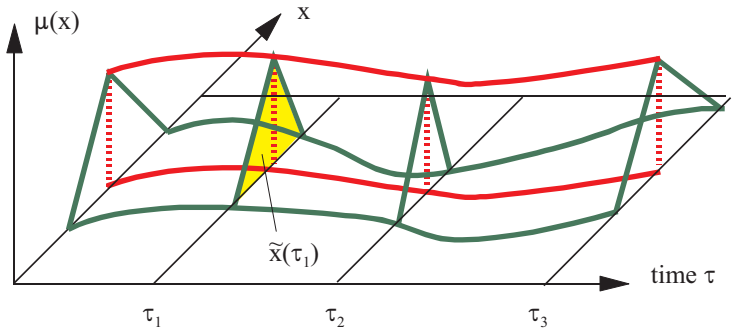

Figure 3: Fuzzy process $\tilde{x}(\tau)$.

$$x(\underline{\tilde{s}},\, \underline{t}) = \tilde{x}(\underline{\tilde{t}}) \tag{6}$$

is applied. Therewith, the fuzziness of both $\tilde{x}$ and $\tilde{t}$ is concentrated in the bunch parameter vector $\underline{\tilde{s}}$.

For each crisp bunch parameter vector $\underline{s} \in \underline{\tilde{s}}$ with the assigned membership value $\mu(\underline{s})$, a crisp function $x(\underline{t}) = x(\underline{s},\, \underline{t}) \in \tilde{x}(\underline{t})$ with $\mu(x(\underline{t})) = \mu(\underline{s})$ is obtained. The fuzzy function

$$\tilde{x}(\underline{t}) = \tilde{x}(\underline{\tilde{s}},\, \underline{t}) = \{(x(\underline{s},\, \underline{t}),\, \mu(x(\underline{s},\, \underline{t}))) \mid \mu(x(\underline{s},\, \underline{t})) = \mu(\underline{s}) \;\; \forall\, \underline{s} \mid \underline{s} \in \underline{\tilde{s}}\} \tag{7}$$

may thus be represented by the fuzzy set of all real valued functions $x(\underline{s}, \underline{t})$ which may be generated from all possible real vectors $\underline{s} \in \tilde{\underline{s}}$. For every $\underline{t} \in \mathbf{T}$, each of the crisp functions $x(\underline{s}, \underline{t})$ yields values x_t which are contained in the associated fuzzy functional values $\tilde{x}_t$. The real functions $x(\underline{s}, \underline{t})$ of $\tilde{x}(\underline{t})$ are referred to as trajectories. Numerical processing of fuzzy functions $\tilde{x}(\underline{t}) = x(\tilde{\underline{s}}, \underline{t})$ demands the discretization of their arguments $\underline{t}$ in space and time.

2.2.2 Fuzzy random function

According to Eqs. (2) and (4), a fuzzy random function is the result of an uncertain mapping

$$\tilde{X}(\underline{t}) : \mathbf{F}(\mathbf{T}) \times \Omega \rightarrow \mathbf{F}(\mathbb{R}). \tag{8}$$

Thereby, **F(X)** and **F(T)** denote the sets of all fuzzy variables in **X** and **T** respectively [14]. At a specific point $\underline{t}$, the mapping of Eq. (8) leads to the fuzzy random variable $\tilde{X}_t = \tilde{X}(\underline{t})$. Therefore, fuzzy random functions are defined as a family of fuzzy random variables

$$\tilde{X}(\underline{t}) = \{\tilde{X}_t = \tilde{X}(\underline{t}) \, \forall \, \underline{t} \mid \underline{t} \in \mathbf{T}\}. \tag{9}$$

For the numerical simulation, again the bunch parameter representation of a fuzzy random function is applied. For each crisp bunch parameter vector $\underline{s} \in \tilde{\underline{s}}$ with the assigned membership value $\mu(\underline{s})$, a real random function $X(\underline{t}) = X(\underline{s}, \underline{t}) \in \tilde{X}(\underline{t})$ with $\mu(X(\underline{t})) = \mu(\underline{s})$ is obtained. The fuzzy random function $\tilde{X}(\underline{t})$ may thus be represented by the fuzzy set of all real random functions $X(\underline{t}) \in \tilde{X}(\underline{t})$

$$X(\tilde{\underline{s}}, \underline{t}) = \{(X(\underline{t}), \mu(X(\underline{t}))) \mid X(\underline{t}) = X(\underline{s}, \underline{t}); \mu(X(\underline{t})) = \mu(\underline{s}) \;\; \forall \, \underline{s} \mid \underline{s} \in \tilde{\underline{s}}\} \tag{10}$$

which may be generated from all possible real vectors $\underline{s} \in \tilde{\underline{s}}$. The real random function $X(\underline{t}) \in \tilde{X}(\underline{t})$ is defined for all $\underline{t} \in \mathbf{T}$ and referred to as original function. A numerical processing of a fuzzy random function $\tilde{X}(\underline{t}) = X(\tilde{\underline{s}}, \underline{t})$ requires the discretization of their arguments $\underline{t}$ in space and time.

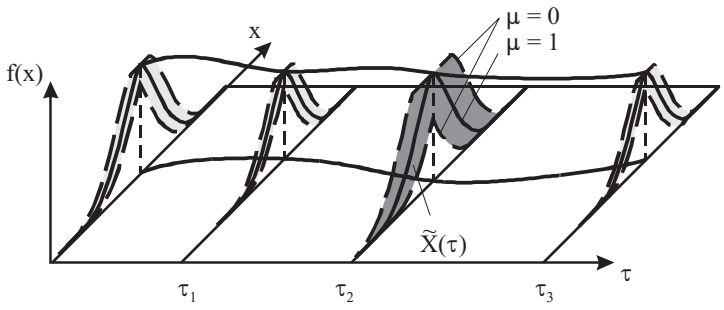

Figure 4: Fuzzy random process $\tilde{X}(\underline{\theta}_j, \tau)$.

3 Fuzzy stochastic analysis

Fuzzy stochastic analysis is an appropriate computational model for processing uncertain data using the uncertainty model fuzzy randomness. Basic terms and definitions related to fuzzy randomness have been introduced, inter alia, by [12]. The formal description of fuzzy randomness chosen by [12] is however not suitable to formulating uncertainty encountered in

engineering tasks. A suitable form of representation with the scope of numerical engineering tasks is given with the so-called α-discretization by [6] and [7].

The numerical simulation under consideration of fuzzy variables and fuzzy functions (fuzzy analysis) may formally be described by the mapping

$$F_{FA}(d): \quad \underline{\tilde{x}}(\underline{t}) \mapsto \underline{\tilde{z}}(\underline{t}). \tag{11}$$

According to Eq. (11), the fuzzy variables $\underline{\tilde{x}}$ and the fuzzy functions $\underline{\tilde{x}}(\underline{t})$ are mapped onto the fuzzy results $\underline{\tilde{z}}(\underline{t})$ with aid of the crisp analysis algorithm d. Every arbitrary deterministic fundamental solution may be used as algorithm d. On the basis of space and time discretization, fuzzy functional values $x(\underline{\tilde{s}},\, \underline{\theta}_j,\, \tau_i,\, \underline{\varphi_k})$ of the function $x(\underline{\tilde{s}},\, \underline{\theta},\, \tau,\, \underline{\varphi})$ are determined at points in space $\underline{\theta}_j$, time τ_i, and a realization of $\underline{\varphi}_k$.

The numerical simulation is carried out with the aid of the α-level optimization [7]. For fuzzy variables $\tilde{x}$ and fuzzy bunch parameter $\underline{\tilde{s}}$ of the fuzzy functions $x(\underline{\tilde{s}},\, \underline{\theta},\, \tau,\, \underline{\varphi})$, an input subspace $\underline{E}_\alpha$ is formed assigned to the level α. By multiple application of the deterministic analysis, the extreme values $z_{\alpha,l}(\underline{\theta}_j,\, \tau_i,\, \underline{\varphi}_k)$ and $z_{\alpha,r}(\underline{\theta}_j,\, \tau_i,\, \underline{\varphi}_k)$ of the fuzzy result variable $\tilde{z}(\underline{\theta}_j,\, \tau_i,\, \underline{\varphi}_k)$ are computed. These points are interval bounds of the α-level sets and enable the numerical description of the convex membership function of the fuzzy result variable $\tilde{z}(\underline{\theta}_j,\, \tau_i,\, \underline{\varphi}_k)$. For the computation of $\tilde{z}(\underline{\theta}_j,\, \tau_{i+1},\, \underline{\varphi}_k)$ at the time point τ_{i+1}, the procedure must be restarted at $\tau = 0$ due to the interaction within the mapping model.

Fuzzy stochastic analysis allows the mapping of fuzzy random input variables onto fuzzy random result variables. The fuzzy stochastic analysis can be applied for static and dynamic structural analysis and for assessment of structural safety, durability as well as robustness. Two different approaches for computation of the fuzzy random result variables have been developed. The first variant (Fig. 5) bases on the bunch parameter representation of fuzzy random variables by [14]. The second variant utilizes the $l_\alpha r_\alpha$-representation of fuzzy random variables. The variant to be preferred depends on the engineering task, the available uncertain data and the wanted results [9].

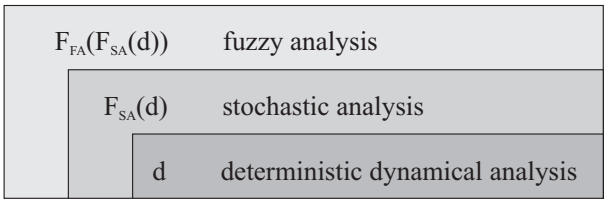

Figure 5: Fuzzy stochastic analysis (FSA).

The fuzzy stochastic analysis is called fuzzy stochastic finite element method (FSFEM), if the deterministic dynamical analysis is based on a finite element (FE) model.

4 DETERMINISTIC DYNAMICAL ANALYSIS OF RC STRUCTURES

4.1 1D – Beams

Plane and spatial beam structures are called 1D-structures. For the physical nonlinear analysis, the cross-sections of the beams are subdivided into layers (plane structures) or fibers (spatial structures). In contrast to the widespread finite element formulations, solutions based on the differential equations for the straight or imperfectly straight beam also exist. A respective approach for plane beam structures is presented here.

The geometrical and physical nonlinear analysis of plane reinforced concrete, prestressed concrete, and steel beam structures is chosen as fundamental model [13]. The beams are subdivided into integration sections, the cross-sections are subdivided into layers. On this basis an incrementally formulated system of second order differential equations for the straight or imperfectly straight beam is solved.

$$\left[\frac{d\Delta\underline{z}(\theta_1)}{d\theta_1}\right]^{[k]}_{(n)} = \underline{A}(\theta_1,\underline{z})_{(n-1)}\cdot\Delta\underline{z}(\theta_1)^{[k]}_{(n)} + \Delta\underline{b}(\theta_1)^{[k-1]}_{(n)} + \underline{d}(\theta_1)_{(n-1)}\cdot\Delta\dot{\underline{z}}(\theta_1)^{[k]}_{(n)} + \underline{m}(\theta_1)_{(n-1)}\cdot\Delta\ddot{\underline{z}}(\theta_1)^{[k]}_{(n)} \quad (12)$$

where $[k]$ – counter of iteration steps; (n) – counter of increments; θ_1 – bar coordinate; Δ – increment; $\underline{z} = \{\underline{z}_1, \underline{z}_2\} = \{u\, v\, \phi; N\, Q\, M\}$ – vector of structural responses; $\underline{A}$ – matrix of coefficients (constant within the increment); $\underline{b}$ – "right hand side" of the system of differential equations with loads and varying parts resulting from geometrical and physical nonlinearities as well as with forces from unbonded prestressing; $\underline{d}$ – damping matrix; and $\underline{m}$ – mass matrix.

The implicit nonlinear system of differential equations for the differential beam sections is linearized by increments. All geometrically and physically nonlinear components in the $\Delta\underline{b}$-vector are recalculated after every iteration step, and the $\underline{A}$-, $\underline{d}$-, and $\underline{m}$-matrix are recalculated after the completion of the iteration within the increment.

The solution of the system of differential equations by a Runge-Kutta integration results in the system of differential equations

$$\underline{K}_{T\,(n-1)}\cdot\Delta\underline{v}^{[k]}_{(n)} + \underline{D}_{T\,(n-1)}\cdot\Delta\dot{\underline{v}}^{[k]}_{(n)} + \underline{M}_{T\,(n-1)}\cdot\Delta\ddot{\underline{v}}^{[k]}_{(n)} = \Delta\underline{P}_{(n)} - \Delta\overset{o}{\underline{F}}{}^{[k]}_{(n)} + \Delta\Delta\underline{F}_{(n-1)} \quad (13)$$

of the unknown incremental displacements $\Delta\underline{v}$, velocities $\Delta\dot{\underline{v}}$, and accelerations $\Delta\ddot{\underline{v}}$ of the nodes.

4.2 2D – folded plate RC structures

Shells, folded plates, shear panels and plates are called 2D-structures. Here, we focus on folded plates which represent the general case for plane 2D structures. They can further be applied to approximate the shape of slightly curved structures. The internal forces are related to the reference plane, which is not stringently the midplane. The cross-section is subdivided into layers to describe the physical nonlinear behavior of reinforced concrete. Over the past years, a new strengthening technology for damaged RC structures has been developed. The thin strengthening layers consist of fine-grained concrete reinforced with textiles made of AR-glass or carbon. The classical layered model with one reference plane for folded plate structures is enhanced to take into account the later applied strengthening layers.

An extended layer model with specific kinematics, the so-called multi-reference-plane model (MRM), is used to describe the load-bearing behavior of RC constructions with textile strengthening. The MRM consists of concrete layers and steel reinforcement layers of the old construction, the strengthening layers comprised of the inhomogeneous material textile concrete (TRC), and the interface layers (Fig. 6). This multilayer continuum has the following kinematic peculiarities. Due to the fact that the modification of the concrete layer thickness is very small and can be neglected, we have $\varepsilon_{33} = 0$. Furthermore, the transverse shear stresses in the concrete layers have no significant influence on the deformation, which means that $\varepsilon_{13} = 0$ and $\varepsilon_{23} = 0$ can be set to zero. The deformation state of the concrete layers may be described by Kirchhoff

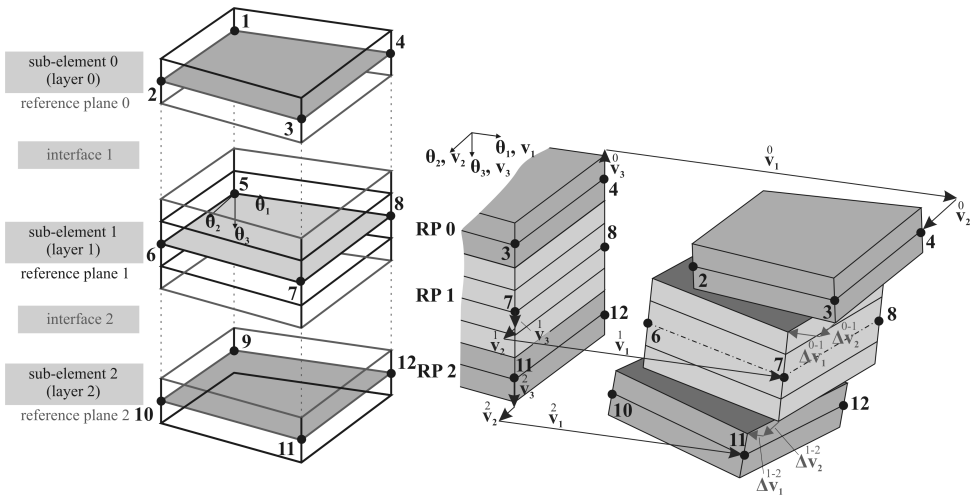

Figure 6: MRM discretization and kinematics.

kinematics. The independent degrees of freedom are assigned to a reference plane which can be selected arbitrarily.

The very thin strengthening layers are subject to the same kinematic assumptions. Kirchhoff kinematics with a reference plane are also assigned to each strengthening layer. The independent degrees of freedom of the strengthening layer lie in the reference plane. The bond between the layers of reinforced concrete and an arbitrary strengthening layer is modeled by an interface. The interface is an immaterial layer of zero thickness. The bonding state is assessed with the help of the relative displacements $\Delta v_1,\ \Delta v_2,\ \Delta v_3$ between the contact surfaces. In conjunction with a bonding matrix, the relative displacements enable assumptions regarding delamination and shear failure.

The FE discretization of the MRM is based on the functional of the complementary energy extended by the static transition conditions $\Delta\underline{p} - \overset{+}{\underline{p}} = 0$ to O_p^r and the equilibrium conditions $\underline{G} \cdot \underline{\sigma}_{el}^e + \overset{+}{\underline{p}}^e - \rho^e \cdot \ddot{\underline{v}}^e = 0$ in V^e

$$\Pi_{mh} = \int_{\tau_1}^{\tau_2} \sum_{e=1}^{n} \left\{ \int_{V^e} \left[w_c(\underline{\sigma}_{el}^e) + (\underline{G} \cdot \underline{\sigma}_{el}^e + \overset{+}{\underline{p}}^e - \rho^e \cdot \ddot{\underline{v}}^e)^T \cdot \underline{v}^e \right] dV + \int_{V^e} (\underline{\sigma}_{el}^e)^T \cdot \underline{\varepsilon}_0^e \, dV \right.$$
$$\left. - \int_{O_p^{r,e}} (\underline{p}^{r,e} - \overset{+}{\underline{p}}^{r,e})^T \cdot \underline{v}^{r,e} dO - \int_{O_v^{r,e}} (\underline{p}^{r,e})^T \cdot \overset{+}{\underline{v}}^{r,e} dO \right\} d\tau \qquad (14)$$

with $w_c(\underline{\sigma}_{el}^e)$ – internal complementary energy; $\underline{G}$ - matrix of differential operators; $\overset{+}{\underline{p}}$ – external forces in V^e ; ρ^e – density in ; $\ddot{\underline{v}}^e$ – internal acceleration in V^e ; ρ^e ; $\underline{\varepsilon}_0^e$ – initial strain; $\underline{p}^{r,e}$ – internal forces in the boundary surface $O_p^{r,e}$; $\overset{+}{\underline{p}}^{r,e}$ – external forces along the boundary surface $O_p^{r,e}$; $\underline{v}^{r,e}$ – displacements of the boundary surface $O_p^{r,e}$; $\overset{+}{\underline{v}}^{r,e}$ – prescribed displacements of the boundary surface $O_v^{r,e}$; τ – time.

After some transformations, the quasi-static part of the equilibrium conditions $(\underline{G} \cdot \underline{\sigma}_{el}^e + \overset{+}{\underline{p}}^e)$

and the kinetic energy become visible in the mixed hybrid functional

$$\begin{aligned}\Pi_{mh} \;=\; \int_{\tau_1}^{\tau_2}\sum_{e=1}^{n}\Bigg\{ & \int_{V^e}\left[w_c(\underline{\sigma}^e_{el}) + (\underline{G}\cdot\underline{\sigma}^e_{el} + \overset{+}{\underline{p}}{}^e)^T\cdot\underline{v}^e + \frac{1}{2}\rho^e\cdot(\dot{\underline{v}}^e)^T\cdot\dot{\underline{v}}^e\right]dV \\ & + \int_{V^e}(\underline{\sigma}^e_{el})^T\cdot\underline{\varepsilon}^e_0\,dV - \int_{O_p^{r,e}}(\underline{p}^{r,e} - \overset{+}{\underline{p}}{}^{r,e})^T\cdot\underline{v}^{r,e}\,dO \\ & - \int_{O_v^{r,e}}(\underline{p}^{r,e})^T\cdot\overset{+}{\underline{v}}{}^{r,e}dO\Bigg\}\,d\tau. \end{aligned} \tag{15}$$

In extension to the static case [8], [18], this functional may be applied to a layered continuum with dynamic loads. Following the procedure described in [8], [18], the steady-state condition of the mixed hybrid functional

$$\delta\Pi_{mh,\,NC} = \frac{1}{2}\,\delta(d^2\Pi_{mh}) = \sum_{i=0}^{k}\delta\left(d^2({}^{(R_i)}\Pi_{mh,\,NC})\right) + \sum_{j=1}^{k}\delta\left(d^2({}^{(I_j)}\Pi_{mh,\,NC})\right) = 0 \tag{16}$$

with

$$\begin{aligned}{}^{(R_i)}\Pi_{mh,\,NC} \;=\; \int_{\tau_1}^{\tau_2}\Bigg\{\sum_{e_i=1}^{n}\Bigg(\frac{1}{2}\sum_{m=0}^{s_i-1}\Bigg[& \int_{V^{e_i,\,m}}(d\underline{\sigma}^{e_i,\,m}_{el})^T\cdot d\underline{\varepsilon}^{e_i,\,m}_{el}dV \\ & + 2\int_{V^{e_i,\,m}}(\underline{G}\cdot d\underline{\sigma}^{e_i,\,m}_{el} + d\overset{+}{\underline{p}}{}^{e_i,\,m})^T\cdot d\underline{v}^{e_i,\,m}dV \\ & + \int_{V^{e_i,\,m}}\rho^{e_i,\,m}\cdot(d\dot{\underline{v}}^{e_i,\,m})^T\cdot d\dot{\underline{v}}^{e_i,\,m}dV \\ & + 2\int_{V^{e_i,\,m}}(d\underline{\sigma}^{e_i,\,m}_{el})^T\cdot d\underline{\varepsilon}^{e_i,\,m}_{0}dV\Bigg] \\ & - \int_{{}^{(R_i)}O_p^{r,\,e_i}}(d\underline{p}^{r,\,e_i} - d\overset{+}{\underline{p}}{}^{r,\,e_i})^T\cdot d\underline{v}^{r,\,e_i}dO \\ & - \int_{{}^{(R_i)}O_v^{r,\,e_i}}(d\underline{p}^{r,\,e_i})^T\cdot d\overset{+}{\underline{v}}{}^{r,\,e_i}dO\Bigg)\Bigg\}\,d\tau \end{aligned} \tag{17}$$

$${}^{(I_j)}\Pi_{mh,\,NC} = \int_{\tau_1}^{\tau_2}\left\{\sum_{e_j=1}^{n}\int_{{}^{(I_j)}O_p^{e_j}}(d^I\underline{\sigma}^{e_j})^T\cdot\left({}^{(j|j)}d\underline{v}^{r,\,e_j} - {}^{(j-1|j)}d\underline{v}^{r,\,e_{j-1}}\right)dO\right\}d\tau \tag{18}$$

for a layered continuum with k layers is obtained from Eq. (15). Eq. (17) describes the functional for the sub-element R_i whereas Eq. (18) depicts the functional for the interface I_j. Compared to [8], [18] Eqs. (16), (17) and (18) are extended by inertial forces. In order to account

for physical nonlinearities of the layered continuum, the layer i with the reference plane R_i is subdivided into s_i sub-layers in Eq. (17).

On the basis of Eq. (16), the differential equation of motion can be derived. Thereby, the same stress shape functions, the same boundary displacement shape functions and the same element displacement shape function are chosen within all layers of the continuum.

The stress shape functions are chosen in such a way, that they fulfil strongly the quasi-static part of the equilibrium conditions

$$\underline{G} \cdot d\underline{\sigma}_{el}^{e_i,m} + d\overset{+}{\underline{p}}^{\,e_i,m} = 0. \tag{19}$$

The evaluation of the steady-state condition, Eq. (16) yields the MRM element and leads to the differential equation of motion

$$\underline{K_T} \cdot d\underline{q} + \underline{M} \cdot d\underline{\ddot{q}} - d\underline{R} - d\underline{R}_K = 0 \tag{20}$$

with $\underline{K_T}$ – tangential system stiffness matrix, $\underline{M}$ – system mass matrix, $d\underline{R}$, $d\underline{R}_K$ – differential load contributions, and $\underline{q}$ – nodal displacement degrees of freedom. The matrix $\underline{K_T}$ and the vectors $d\underline{R}$, and $d\underline{R}_K$ are identical to the corresponding values of the hybrid procedure in [8]. The system mass matrix $\underline{M}$ is specified in [17].

4.3 3D – compact RC structures

Hybrid eight-node hexagonal solid elements for the physical linear static analysis are described in [11]. For the physically nonlinear analysis of reinforced concrete and textile reinforced concrete (TRC), respectively, two kinds of reinforcement are introduced – single fibers and fiber layers (see Fig. 7). The formulation of the hybrid eight-node hexagonal solid element with embedded (textile) reinforcement is outlined in the following.

Starting point is the functional of Hellinger-Reissner

$$\Pi_{HR} = \int_V \left(\underline{\sigma}^T \cdot (\underline{G} \cdot \underline{v}) - \frac{1}{2}\underline{\sigma}^T \cdot \underline{\varepsilon} - \overset{+}{\underline{p}}{}_V^T \cdot \underline{v} \right) dV - \int_{O_p} \overset{+}{\underline{p}}{}^T \cdot \underline{v}\, dO \tag{21}$$

with $\underline{\sigma}$, $\underline{\varepsilon}$, $\underline{v}$ – stresses, strains and displacements in the volume V, $\overset{+}{\underline{p}}{}_V^T$ – external forces in V and $\overset{+}{\underline{p}}{}^T$ – external forces along the boundary surface O_p, and the matrix of differential operators $\underline{G}$.

Based on it, the Hamilton functional is build

$$H = \delta \int_{\tau_1}^{\tau_2} (K - \Pi_{HR})\, d\tau = \delta \int_{\tau_1}^{\tau_2} \left(\frac{1}{2} \int_V \rho \cdot (\dot{v})^T \cdot \dot{v}\, dV - \Pi_{HR} \right) d\tau \tag{22}$$

with the kinetic energy K.

The physical nonlinear analysis of reinforced concrete is a non-conservative problem arising e.g. from crack formation, nonlinear material behavior, bonding and damage. In order to solve this non-conservative problem, a differential load change is considered. Under such load change, the existence of a potential is assumed. The differential load change leads to a transition of the structure from the basic condition to a differentially adjacent neighboring condition (NC). The steady-state condition of the neighboring condition is therefore

$$\delta H_{NC} = \frac{1}{2}\delta(d^2 H) = 0 \tag{23}$$

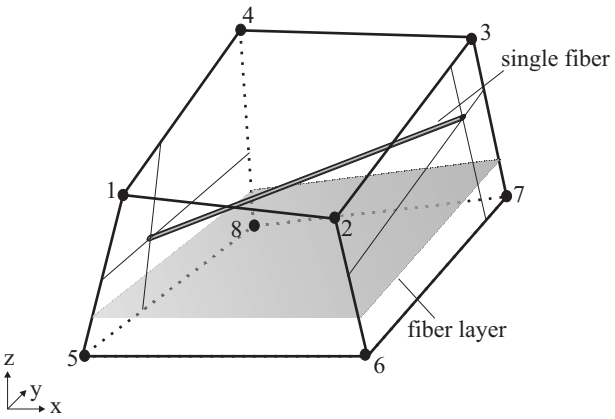

Figure 7: Eight-node solid element with embedded reinforcements.

with

$$H_{NC} = \int_{\tau_1}^{\tau_2} \left(\frac{1}{2} \int_V \rho \cdot (d\dot{\underline{v}})^T \cdot d\dot{\underline{v}} \, dV - \int_V \left(d\underline{\sigma}^T \cdot (\underline{G} \cdot d\underline{v}) - \frac{1}{2} d\underline{\sigma}^T \cdot d\underline{\varepsilon} - d\underline{p}^+_V{}^T \cdot d\underline{v} \right) dV + \int_{O_p} d\underline{p}^+{}^T \cdot d\underline{v} \, dO \right) d\tau. \tag{24}$$

The continuum is subdivided into n finite 3D elements. The volume V^e of one finite 3D element e consists of the matrix volume V_m^e and the reinforcement volume V_b^e. Single fibers (sf) and fiber layers (fl) are taken into account. The volume of the reinforcement V_b^e consists then of n_{sf} single fibers and n_{fl} fiber layers. For a function F (e.g. stresses, strains, displacements) holds

$$\begin{aligned} \int_{V^e} F dV &= \int_{V_m^e} F_m dV + \int_{V_b^e} F_b dV = \int_{V^e} F_m dV + \int_{V_b^e} F_b dV - \int_{V_b^e} F_m dV \qquad (25) \\ &= \int_{V^e} F_m dV + \sum_{i=1}^{n_{sf}} \int_{V_{sf}^{e,i}} F_{sf}^{e,i} dV + \sum_{j=1}^{n_{fl}} \int_{V_{fl}^{e,j}} F_{fl}^{e,j} dV - \sum_{i=1}^{n_{sf}} \int_{V_{sf}^{e,i}} F_m^{e,i} dV - \sum_{j=1}^{n_{fl}} \int_{V_{fl}^{e,j}} F_m^{e,j} dV. \end{aligned}$$

With Eq. (25), the reinforcement is taken into account in Eq. (24)

5 MODEL REDUCTION

The computational cost of a fuzzy stochastic structural analysis of RC structures under dynamic loads is almost completely caused by the nonlinear FE analysis. Thus, the most effective measure to increase the numerical efficiency is to replace the costly deterministic computational model (innermost loop in Fig. 5) by a fast approximation solution based on a reasonable amount of initial deterministic computational results. The fuzzy stochastic analysis can then be performed with that surrogate model, which enables the utilization of an appropriate sample size for the simulation. The surrogate model is designed to describe a functional dependency between the structural parameters $\underline{x}$ and the structural responses $\underline{z}$ in the form of a response surface approximation

$$\underline{z} = f_{RS}(\underline{x}). \tag{26}$$

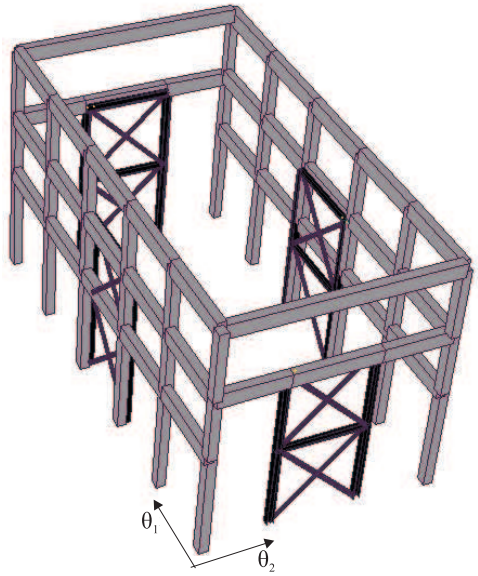

Figure 8: 3D pictorial view of the upgraded structure with scheme of the bracing system configuration.

For response surface approximation a variety of options exist (see [10], [16]). The suitability of the particular developments primarily depends on the properties of the computational model. Due to the very general properties of the FE analysis in structural analysis of textile strengthened RC structures, which can hardly be limited to convenient cases, a high degree of generality and flexibility of the approximation is demanded. In this context, an artificial neuronal network provides a powerful basis for response surface approximation. This approach can extract information from initial deterministic computational results and can subsequently reproduce the structural response based on the extracted information only. According to the universal function approximation theorem, artificial neural networks are capable of uniformly approximating any kind of nonlinear functions over a compact domain of definition to any degree of accuracy. There is virtually no restriction for a response surface approximation with the aid of artificial neural networks.

In the case, that the global structural behavior is dominated from few eigen modes, the number of degrees of freedom can be reduced. In the following example, a simplified 2-DOF model is used as equivalent system for the whole structure.

6 EXAMPLE

6.1 Investigated structure

The investigated building (Fig. 8) has a rectangular plan whose dimensions are $10.80 \times 20.40\,\mathrm{m}^2$. The elevation of the first floor is 7.40 m, whereas the second one is at 11.10 m. It is characterized by a RC structure framed in the longitudinal direction only and is designed against vertical loads without account for seismic action. Columns and beams have rectangular $40 \times 50\,\mathrm{cm}^2$ and $40 \times 70\,\mathrm{cm}^2$ cross-sections, respectively. The T-shaped hollow tile RC floors have a 6 cm thick concrete slab, so that the total depth of the first floor is 36 cm, whereas the second, at the roof level, is 30 cm.

In [4], the results of the vulnerability evaluation have been published. Thereby, a three-dimensional FEM model with beam elements of the structure has been created considering

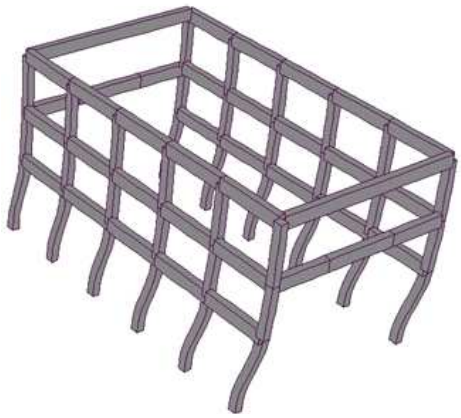

Figure 9: Deformed shapes of the fundamental vibration modes for one principal directions.

floors like rigid diaphragms in the horizontal plane. Two nonlinear static analyses and a set of linear and nonlinear time history analyses have allowed to evaluate the vulnerability of the structure in the as-built condition and the effectiveness of the upgrading interventions. First of all, a calculation of the natural frequencies of the system has been carried out. Relevant values are 2.075 s^{-1} in Θ_1 direction (longitudinal, see Fig. 9) and 0.796 s^{-1} in Θ_2 direction (transverse). The mass participation factors are higher than 95% for such modes, so that the structure can be assumed as a matter of fact as made of two mutually independent SDOF systems in both Θ_1 and Θ_2 direction. This consideration assumes relevance in the determination of the optimal value of the damping devices. In fact, a design procedure for viscous devices based on simplified 2-DOF system can be used when the structural dynamic behavior can be interpreted through two SDOF systems [1], [5].

A peak ground acceleration (PGA) of 0.25 g has been assumed in the analysis, considering the combination of site effect and the importance of the structure regard to collapse.

The time history analysis has shown an excessive deformability of the original structure, not compatible with the structural safety and immediate occupancy requirement after seismic events [2], [3]. The assumed upgrading interventions are aimed at reducing the lateral floor displacements of the structure by means of steel braces fitted with additional energy dissipation devices. Such devices connect the original structure at the first floor level with rigid steel braces and act due to the relative displacements occurring between the original structure and the steel braces. The study, presented in this paper, has been carried out considering the connection with purely viscous devices. As shown in [4], the reduction of horizontal floor displacements obtained thanks to the addition of this kind of devices is greater than the one obtained with a rigid connection of the original structure to the steel braces.

6.2 Uncertain input parameters

No technical documentation regarding the history of the structure is available, apart from the period of erection, which can be dated at the end of the 60s of XX century, on the basis of oral testimony.

Because of the lack of technical data and in order to find information about, the quality of structural materials, some characterization tests have been carried out on concrete core bored specimens and steel bars taken out of the structure. In result of the tests, the mechanical resistance of concrete is evaluated by means of fuzzy quantities. The concrete compressive and

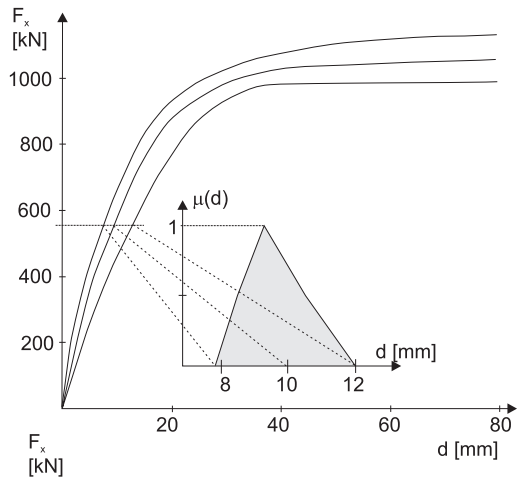

Figure 10: Fuzzy load-displacement dependency of the existing RC frame structure.

tensile strength are modeled as fuzzy triangular numbers $\tilde{\mathrm{f}}_{\mathrm{ck}} = \langle 14,\, 16.5,\, 20\rangle\,\mathrm{N/mm^2}$ and $\tilde{\mathrm{f}}_{\mathrm{t}} = \langle 1.5,\, 2.0,\, 2.5\rangle\,\mathrm{N/mm^2}$, respectively. A magneto-metric survey has been also carried out in order to locate the position and the diameter of steel bars in beams and columns. For the numerical study, twelve steel bars with a fuzzy cross-sectional area $\tilde{\mathrm{A}} = \langle 2.69,\, 3.14,\, 3.21\rangle\,\mathrm{cm^2}$ are considered. In order to assess the seismic vulnerability of the existing structure, nonlinear static analyses have been carried out under consideration of fuzzy resistance variables. The response of the as-built structure along both principal directions has then been evaluated in terms of fuzzy capacity curves F-d (Fig. 10). These curves have been represented in an approximate way by means of equivalent SDOF nonlinear relationships. Thereby, the kernel curve with $\mu\left(d(F)\right) = 1$ is scaled according to

$$\tilde{d}(F) = {}_{1.0}d(F) + \tilde{a} \cdot F \tag{27}$$

with $\tilde{\mathrm{a}} = \langle -3.3,\, 0.0,\, 6.0\rangle\, 10^{-3}$. The steel braces are also modeled as SDOF system with fuzzy stiffness $\tilde{\mathrm{K}}$ and fuzzy mass $\tilde{\mathrm{M}}$. Two variants are investigated especially: Variant 1 $\tilde{\mathrm{K}}_1 = \langle 39,\, 40.8,\, 43\rangle$ MN/m with $\tilde{\mathrm{M}}_1 = \langle 1.1,\, 1.3,\, 1.5\rangle$ t and Variant 2 $\tilde{\mathrm{K}}_1 = \langle 50,\, 52.5,\, 55\rangle$ MN/m with $\tilde{\mathrm{M}}_1 = \langle 1.2,\, 1.55,\, 1.8\rangle$ t. The uncertainty of the viscosity $\mathrm{c_x}$ of the connecting devices is with a fuzzy scaling factor according to $\tilde{\mathrm{c}} = \tilde{\mathrm{b}} \cdot \mathrm{c_x}$ with $\tilde{\mathrm{b}} = \langle 0.9,\, 1.0,\, 1.1\rangle$.

6.3 Fuzzy structural analysis

Nonlinear time-history analyses of the simplified 2-DOF system have then been performed considering the seismic input of Taiwan (1999) earthquake, scaled to PGA value of 0.25 g. Fig. 11 displays the time-history of the ground acceleration of the Taiwan earthquake. The fuzzy maximum displacement $\tilde{v}_{TD}$ at the top of the structure has been calculated on the basis of the fuzzy displacement-time dependency, as shown for one realization in Fig. 12. The parameter study with variation of the viscosity of damping devices yields a fuzzy function $\tilde{v}_{TD}(c_x)$ as presented in Fig. 13 for the Taiwan earthquake.

ACKNOWLEDGMENTS

Authors gratefully acknowledge the support of the German Research Foundation (DFG) within the framework of the Collaborative Research Center (SFB) 528 and the contribution of Alberto Mandara (Second University of Naples).

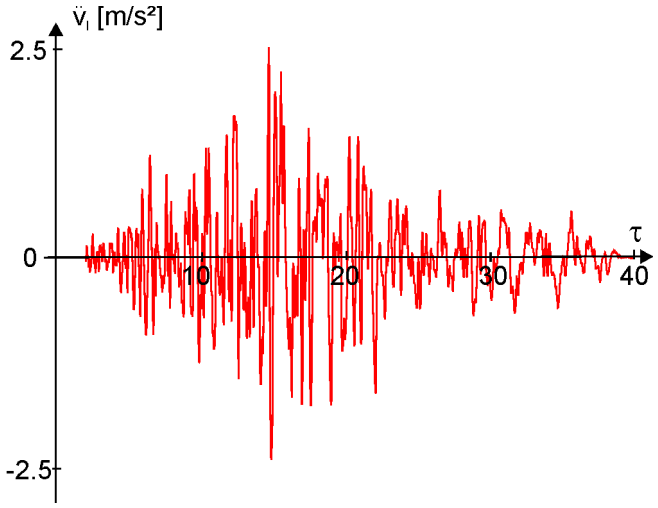

Figure 11: Acceleration of the Taiwan earthquake scaled to PGA value of 0.25 g.

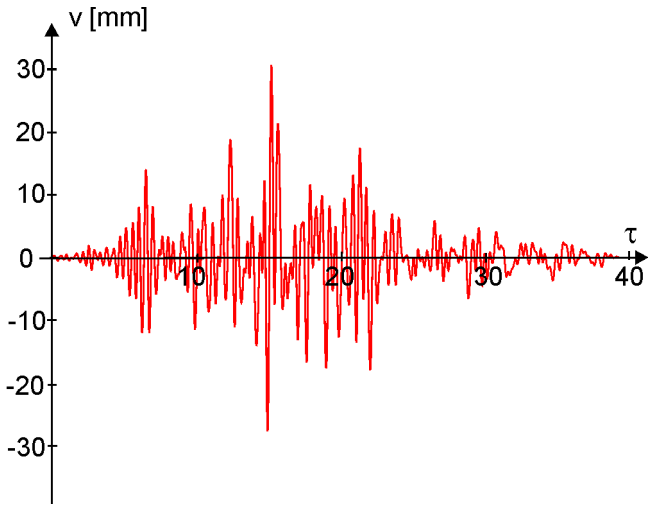

Figure 12: Realization of the fuzzy displacement-time dependency due to the Taiwan earthquake.

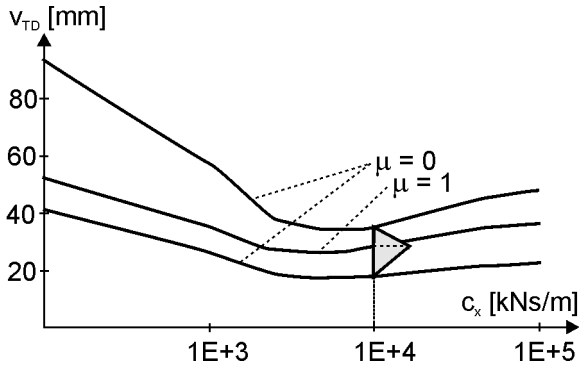

Figure 13: Fuzzy top displacement in dependency of the viscosity.

REFERENCES

[1] A. Mandara, F.M. Mazzolani, On the Design of Retro-fitting by means of Energy Dissipation Devices. *7th International Seminar on Seismic Isolation, Passive Energy Dissipation and Active Control of Vibrations of Structures*, Assisi, 2001.

[2] A. Mandara, F. Ramundo, G. Spina, Seismic up-grading of an existing r.c. building by steel braces and energy dissipation devices. *XXI National Congress of CTA*, Catania, 2007.

[3] A. Mandara, F. Ramundo, G. Spina, Steel Bracing for the Optimal Seismic Control of Existing r.c. Structures. *5th European Conference on Steel and Composite Structures*, Graz, 2008.

[4] A. Mandara, F. Ramundo, G. Spina, Seismic up-grading of r.c. structures with innovative bracing systems. *Proceedings of PROHITEC*, London, 2009.

[5] F.M. Mazzolani, A. Mandara, Seismic up-grading of an Old Industrial Building by Dissipative Steel Roofing. *International Seminar on Structural Analysis of Historical Constructions*, Padova, 2004.

[6] B. Möller, M. Beer, *Fuzzy Randomness – Uncertainty in Civil Engineering and Computational Mechanics*, Springer, Berlin, 2004.

[7] B. Möller, W. Graf, M. Beer, *Fuzzy structural analysis using α-level optimization*. Computational Mechanics, **26**, 547–565, 2000.

[8] B. Möller, W. Graf, A. Hoffmann, F. Steinigen, *Numerical simulation of RC structures with textile reinforcement*. Computers and Structures, **83**, 1659–1688, 2005.

[9] B. Möller, W. Graf, J.-U. Sickert, U. Reuter, *Numerical simulation based on fuzzy stochastic analysis*. Mathematical and Computer Modelling of Dynamical Systems, **13**, 349–364, 2007.

[10] R. H. Myers, D. C. Montgomery, *Response Surface Methodology: Process and Product Optimization Using Designed Experiments*, Wiley, New York, 1995.

[11] H.H.T. Pian, C.-C. Wu, *Hybrid and incompatible finite element methods*, Champman and Hall, Boca Raton, 2006.

[12] M.L. Puri, D. Ralescu, *Fuzzy random variables*. Journal of Mathematical Analysis and Applications, **114**, 409–422, 1986.

[13] R. Schneider, *Stochastische Analyse und Simulation des nichtlinearen Verhaltens ebener Stabtragwerke mittels M-N-Q-Interaktionsmodell*. Dissertation, Technische Universität Dresden, Veröffentlichungen des Lehrstuhls für Statik, Heft 2, 2001.

[14] J.-U. Sickert, M. Beer, W. Graf, B. Möller, *Fuzzy probabilistic structural analysis considering fuzzy random functions. 9th International Conference on Applications of Statistics and Probability in Civil Engineering*, Rotterdam, Millpress, 2003.

[15] J.-U. Sickert, *Fuzzy-Zufallsfunktionen und ihre Anwendung bei der Tragwerksanalyse und Sicherheitsbeurteilung*. Dissertation, Technische Universität Dresden, Veröffentlichungen Institut für Statik und Dynamik der Tragwerke, Heft 9, 2005.

[16] T. Simpson, J. Poplinski, P. N. Koch, J. Allen, *Metamodels for computer-based engineering design: Survey and recommendations.* Engineering with Computers, **17**, 129-150, 2001.

[17] F. Steinigen, B. Möller, W. Graf, A. Hoffmann, *Numerical simulation of textile reinforced concrete considering dynamic loading process*. J. Hegger, W. Brameshuber, N. Will, editors, *Textile Reinforced Concrete Proceedings of the 1st International RILEM Conference*, Aachen, 2006.

[18] F. Steinigen, *Numerische Simulation des Tragverhaltens textilverstärkter Bauwerke*. Dissertation, Technische Universität Dresden, Veröffentlichungen Institut für Statik und Dynamik der Tragwerke, Heft 11, 2006.